Analysis of Normal Shock Noise Measurements on Nose-Cylinder Bodies

J. PETER READING* AND ROLF A. GUENTHER†
Lockheed Missiles & Space Company Inc., Sunnyvale, Calif.

Fluctuating pressure measurements at transonic speed have been obtained for three nose-cylinder configurations (15° cone cylinder, biconic nose-smooth cylinder, and biconic corrugated cylinder). Special emphasis was placed on determining both the steady and unsteady flow environment produced by the terminal normal shock wave and its associated separated flow bubble. This was accomplished by locating boundary-layer profile surveys near the separation bubble and by having a high density of fluctuating pressure transducers in the same vicinity. The data revealed both a rippling of the shock lambda and a circumferential variation of the boundary-layer thickness aft of reattachment. The coherence in the separated region has a peak which compared reasonably well with the predicted resonant frequency of the separation pocket based on Trilling's two-dimensional incident shock model. It is concluded, therefore, that the separated flow region must consist of three-dimensional cells in order to be consistent with these and other experimental results. A flow model having the following characteristics is postulated: In the central portion of the cell the flow resembles the classical two-dimensional recirculatory bubble, but each cell is vented by a pair of counterrotating vortices which start at the surface and flow downstream.

Nomenclature

a	= speed of sound, m/sec
c	= reference length (cylinder diameter), 0.544m
C_p	= pressure coefficient, $(p - p_\infty)/q$
ΔC_p(rms)	= root mean square fluctuating pressure coefficient
d	= cylinder diameter, m
f	= frequency, Hz
h	= average width of corrugation face, m
H	= boundary-layer shape factor, δ^*/θ
l_s	= length of separated region, m
M	= freestream Mach number, U_∞/a
$P_{1,2}$	= amplitude of cross power spectral density at a given frequency
p	= pressure, kg/m²
q	= dynamic pressure, kg/m²
R_c	= Reynolds number based on cylinder diameter
R_e	= unit Reynolds number, 1/m
FPL	= fluctuating pressure level, db
U	= local velocity, m/sec
U_e	= boundary-layer edge velocity, m/sec
$\bar{U}$	= average recirculation velocity, m/sec (Ref. 8)
U_∞	= freestream velocity, m/sec
x	= axial coordinate, origin at nose of biconic model, m
y	= coordinate normal to model surface, m
α	= angle of attack, deg
$\gamma_{1,2}{}^2$	= coherence function, $\gamma^2{}_{1,2}(x, f) = \lvert P_{1,2}(x, f)\rvert^2/P_1(x, f) P_\theta(x, f)$; (Ref. 1)
δ^*	= boundary-layer displacement thickness, m
θ	= boundary-layer momentum thickness, m
ϕ	= azimuth angle measured from leeward meridian, deg
ω	= circular frequency, rad/sec
∞	= freestream conditions
1, 2	= measuring station index

Presented as Paper 72-669 at the AIAA 5th Fluid and Plasma Dynamics Conference, Boston, Mass., June 26–28, 1972; submitted June 28, 1972; revision received February 8, 1973. This analysis was accomplished in part under NASA Contract NAS 8-21459. The authors are indebted to E. J. Lukus and J. T. Huang, who conducted the experiments and supervised the data reduction, and to G. A. Wilhold and P. W. Howard of NASA Marshall Space Flight Center for making available much of the instrumentation used in the experiments.

Index categories: Aircraft Vibration; Nonsteady Aerodynamics; Subsonic and Transonic Flow.

* Research Specialist. Member AIAA.
† Senior Aerodynamics Engineer.

Introduction

AERODYNAMIC pressure fluctuations can be an important factor in booster design since they can cause panel flutter, excite a bending mode, or subject a sensitive payload to an excessive noise environment. As yet, theoretical techniques are imperfect, particularly for complicated configurations (e.g., the biconic nose corrugated cylinder configuration shown in Fig. 1), and one must rely on experiments. Thus, fluctuating pressure measurements were obtained in the Arnold Engineering Development Center Propulsion Wind Tunnel (16 T). A complete description of the facility can be found in Ref. 2. However, experiments must be scaled to predict the flight vehicle environment, and a good understanding of the flow mechanism causing the noise is vital to ensure proper simulation. The present paper presents an analysis of the fluctuating pressure environment on three nose cylinder configurations (Fig. 1). The analysis was aimed at gaining a better understanding of the physical phenomena that affect pressure fluctuations at the foot of the normal shock.

Verification of Results

Wind-tunnel fluctuating pressure results are always somewhat in question owing to the usually unknown influence of tunnel background noise. The present results are no exception. The background noise spike at 630 Hz dominates the

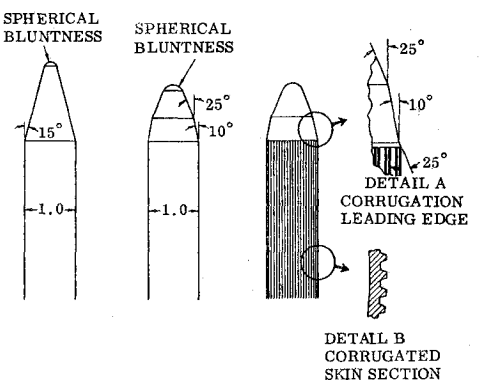

Fig. 1. Model configurations.

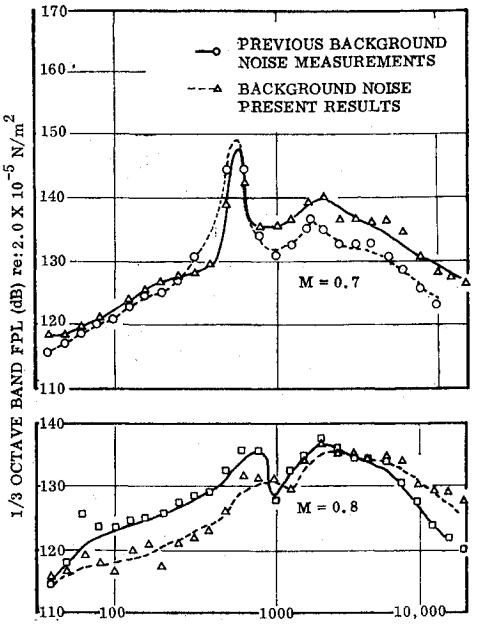

Fig. 2 Comparison of background noise spectra, $R_c = 6.5 \times 10^6$.

frequency spectra aft of the cone-cylinder shoulder at $M = 0.7$ (Fig. 2). Comparison of spectra obtained on the 15° nose cone with previous background noise spectra[3] verifies that this is indeed characteristic of the tunnel. However, it has vanished by $M = 0.8$ (Fig. 2). At $M \leq 0.75$, where the extraneous noise dominates the spectra, the over-all fluctuating pressure does not scale with dynamic pressure as it should if it were due to the tunnel boundary layer. Thus, the $M \leq 0.75$ and $R_e = 5.9 \times 10^6$/m results are probably invalidated by an extraneous noise of mechanical origin.

The blunted 15° cone-cylinder has received some attention from Coe,[4] thus giving a basis of comparison to help determine the validity of the present measurements. The agreement with Coe's results[4] under the shock is encouraging, but the agreement deteriorates badly downstream (Fig. 3). The differences between the present results and Coe's data far aft of the normal shock are rather surprising since in both cases the boundary layer is turbulent and one would not expect such large differences. The reasons for the differences have not been definitely resolved; however, one is able to draw some inferences from the data. The unusual fluctuating pressure distribution of the present results scales with dynamic pressure. The distribution is also sensitive to the cylinder structure. The fluctuating pressure distribution aft of the shcok is relatively

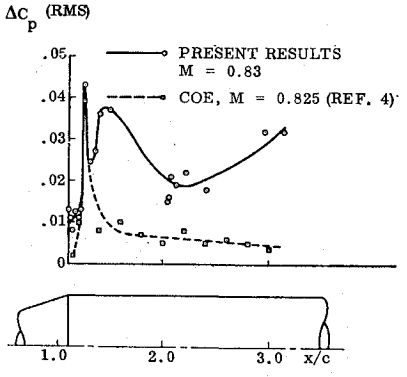

Fig. 3 Comparison of Results, 15° cone-cylinder, $M = 0.83$, $\alpha = 0$.

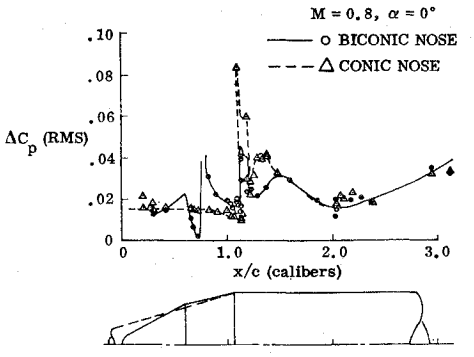

Fig. 4 Effect of nose configuration, $M = 0.8$, $\alpha = 0$.

unaffected by the nose configuration if the cylinder is smooth (Fig. 4), but the high noise levels at $x/c = 1.65$ and 3.05 are substantially reduced when the cylinder is stiffened with corrugations (as shown in Fig. 5). Furthermore, the over-all fluctuating pressure level aft of the shock disturbance on the corrugated cylinder does not agree too badly with Coe's measurement (compare Figs. 3 and 5), considering that the corrugations should increase the fluctuating pressure level due to higher shear in the boundary layer. Distribution minima on the smooth cylinder correspond to model bulkhead locations ($x/c = 1.088$ at the shoulder and $x/c = 2.42$ and 3.76), while maxima occur at antinode locations (Figs. 4 and 5). The conclusion is obvious: the model shell must have been vibrating and the transducers were responding to accelerations or the resulting flow perturbations, or both. The reason the shock-induced pressure fluctuation measurements appear relatively unaffected is because the shock lies nearly on top of the

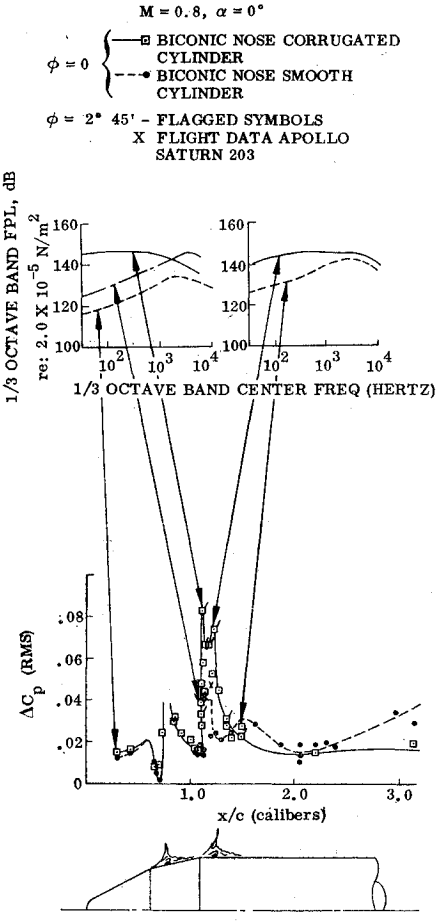

Fig. 5 Effect of cylinder corrugations, $M = 0.8$, $\alpha = 0$.

shoulder bulkhead for $0.8 \leq M \leq 0.9$, and the low-frequency shock does not respond well to the high-frequency model vibrations. Thus, over the cylinder, only the fluctuating pressure measurements under the normal shock for $0.8 \leq M \leq 0.9$ are considered valid.

Discussion of Results

The flowfield over a biconic nose at high subsonic speeds is unique since two normal shocks can exist in succession. The first occurs just aft of the cone-cone shoulder; and the second, if the expansive turning is great enough, occurs aft of the nose-cylinder juncture. The first shock acts as a boundary-layer bleed. The low energy portion of the boundary layer is trapped in the separated region at the foot of the shock. Thus, the boundary layer downstream is strengthened, i.e., can negotiate a greater pressure gradient. Ericsson[5] has shown that this preseparation effect prevents the on-off separation observed by Chevalier and Robertson[6] on cone-cylinders, which can result in aerodynamic undamping and possible aeroelastic instability of the low-frequency modes of an elastic launch vehicle. This low-energy flow is eventually scavenged downstream in longitudinal vortices (as will be discussed in detail later) which also play a part in energizing the boundary layer downstream of the shock. The result is a reduced fluctuating pressure spike aft of the cone-cone shoulder and a decreased separation bubble length (Fig. 4).

Even though the models were quite large, it was necessary to use data from various circumferential positions to get a complete fluctuating pressure distribution under the bubble. This could give an erroneous indication of the axial fluctuating pressure distribution since the normal shock ripples circumferentially (as will be discussed in detail later). Fortunately, the microphones at one circumferential position on the corrugated model appear to have caught the salient features of the fluctuating pressure distribution under the mormal shock (Fig. 5). (The validity of these measurements is further verified by the close agreement with flight data for a 25–12.5° biconic nose). The double-humped noise distribution is similar to that observed on hammerhead configurations.[7] The first sharp peak is the result of the separation shock, and the broader second hump results from the relatively diffuse reattachment. Examination of the spectra at the stations indicated in Fig. 5 confirms this.

Forward of the shock the spectrum is similar to the undisturbed boundary layer on the fore-cone, but is elevated owing to the effects of the corrugations and the upstream effect (through the sublayer) of the shock. Under the forward leg of the lambda shock, the spectrum shows the typical low-frequency content which tends to dominate the separated region. The reattachment zone spectrum shows relatively more

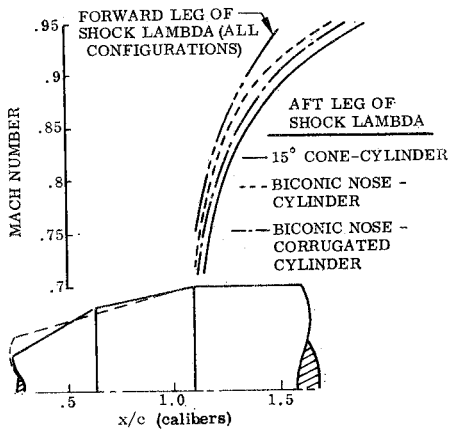

Fig. 6 Effect of nose configuration on extent of shock lambda.

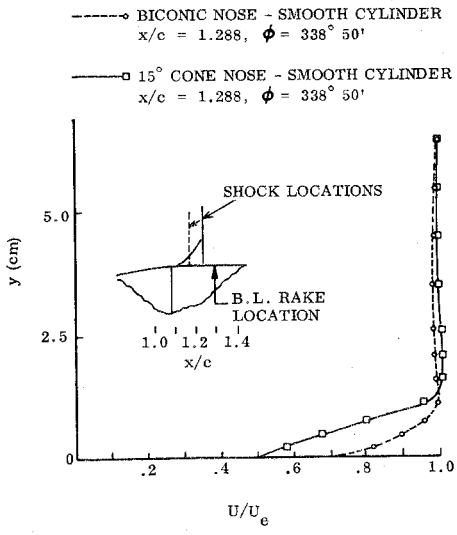

Fig. 7 Boundary-layer profiles aft of reattachment, $M = 0.8$, $\alpha = 0$.

energy at the higher frequencies. Aft of reattachment, the spectrum is similar to the elevated turbulent boundary layer which exists forward of separation.

The effect of the biconic nose on the extent of separation is verified from schlieren measurements of the shock lambda (Fig. 6). Within the accuracy of the schlieren photographs the forward leg of the shock lambda appears to be fixed relative to the shoulder for all three configurations, and the location of the aft leg is sensitive to configuration changes. The largest extent of the shock lambda occurs for the 15° cone-cylinder model. The biconic nose causes a contraction of the lambda while the corrugated skin increases its spread. Thus, the schlieren results agree with the fluctuating pressure results discussed earlier. Likewise, boundary-layer profile measurements show a more filled-out velocity profile for the biconic nose than for the 15° nose at the same station aft at the shoulder (Fig. 7). The greater velocity deficit in the 15° cone-cylinder boundary layer is probably a remnant of separation. That is, the boundary layer has not yet recovered to a fully developed turbulent profile. It would appear that reattachment is closer to the measuring station on the 15° cone-cylinder model —further evidence that the biconic nose reduces the extent of separation. Incidentally, the boundary-layer survey results indicate that separation does indeed occur forward of the measuring station for the 15° cone-cylinder (Fig. 8). Unfortunately, the fixed rake positions missed the separation region on the biconic nose.

The coherence function under the separation pocket reveals that the fluctuating pressure there appears to be affected by a variety of flow phenomena (Fig. 9). Trilling[8] has shown that a resonant condition can exist in the separation pocket under an incident wave. Using his lowest harmonic ($\omega l_s/\overline{U} = 1.79$) gives a resonant frequency of 1400 to 1900 Hz. (The frequency spread is due to the uncertainty in measuring the length of

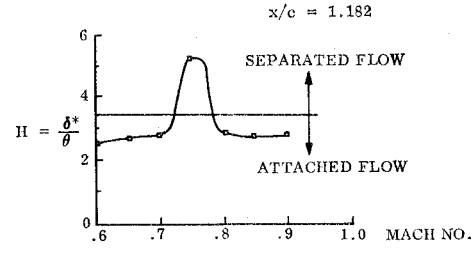

Fig. 8 Boundary-layer shape parameter measurements, 15° cone-cylinder.

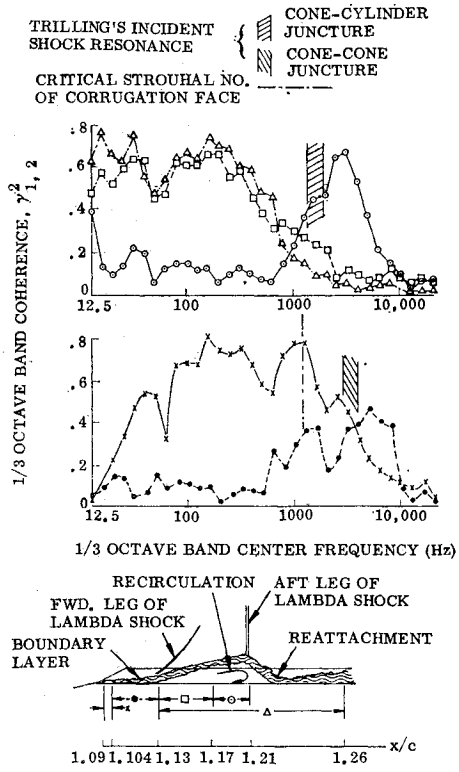

Fig. 9 Coherence measurements in a corrugation valley, $M = 0.8$, $\alpha = 0$, $\phi = 2° 45'$.

the separation bubble.) The high coherence observed between two points under the separation bubble ($x/c = 1.21$ and 1.17) seems to indicate that the bubble does indeed resonate at about Trilling's resonant frequency (Fig. 9). Thus, Trilling's two-dimensional flow model seems to predict the pocket resonance reasonably well. Ordway[9] has shown that the vorticity shed by a rectangular rod with one face normal to the flow may be predicted by the critical Strouhal frequency of a cylinder ($\omega d/U_\infty = 0.2$) if the cylinder diameter d is substituted with 1.7 h, where h is the width of the face normal to the flow. Using the average width of the forward face of the corrugation for h gives a shedding frequency of 1150 Hz. Thus, the peak coherence of about $\gamma^2_{1,2} = 0.8$ between adjacent points just aft of the corrugation leading edge ($x/c = 1.09$ and 1.104) is probably the result of the vorticity emanating from the corrugation leading edge. Both the boundary-layer flow and the forward edge of the shock lambda seem to be somewhat affected by the vorticity shed by the corrugation leading edge and, possibly, by the resonance of the forward separation pocket at the cone-cone shoulder. This is demonstrated by the moderate peaks in coherence for the essentially uncorrelated pressure fluctuations between $x/c = 1.104$ and 1.13. These remnants of the upstream flow appear to leave the corrugation valley, as demonstrated by the poor high-frequency correlation coefficient between the forward leg of the shock lambda and the separation bubble (between $x/c = 1.13$ and 1.17) and between separation and reattachment ($x/c = 1.13$ and 1.26).

This scavenging of the valley flow is the result of the earlier expansion of the flow into the valley (Fig. 10). Since the valley shoulder precedes the corrugation shoulder, lower pressures occurs in the valley adjacent to the relatively high pressures along the ramp at the corrugation leading edge. Thus, the ramp flow spills into the valley. At the corrugation shoulder, reduced pressures are achieved by the flow expanding around the corner from the ramp. Meanwhile, the pressures in the valley adjacent to the shoulder have recovered somewhat. The result is a lower pressure at the corrugation top than in

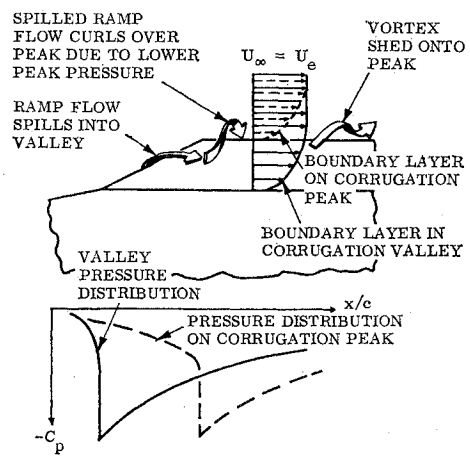

Fig. 10 Generation of vorticity at corrugation edges.

the valley; therefore, the flow is out of the valley, curling up onto the corrugation top. The direction of the shear between the boundary layer developed in a corrugation valley and the boundary layer developed over a corrugation top tends also to produce vorticity which curls up over the corrugation top. That is, a finite velocity will occur over the center of the valley at a height above the valley floor equal to the corrugation height. Zero velocity will occur at the corrugation top. The resulting vorticity produces a transverse flow component that will be in the direction of the corrugation top.

The present results seem to indicate a classical two-dimensional separation (Trilling's model is two dimensional) with some three-dimensional vorticity superimposed by the corrugations. However, there is a great deal of evidence that two-dimensional separations are hard to achieve. Many investigators have observed cellular or vortical flow patterns in various kinds of flow separation (e.g., in laminar and turbulent reattaching flow,[10,11] in regions of turbulent shock or step-induced separation,[12-14] in separated regions on wings,[15] in regions of nose-induced separation on bodies of revolution[13]). Ginoux[16] has shown that concave flows can re-establish lingering traces of vorticity within the boundary layer and expand them to significant proportions. Tobak[17] and Persen[18] see this as the basic mechanism behind the ablation crosshatching phenomenon. Persen even sees streamwise vorticity as a fundamental concept in all fluid flows.[19] This is further verified by the experimental work of Zakkay and Calarese.[20] Thus, the vortical nature of separated flows and the magnification of remnant vorticity by concave flows is well recognized. Furthermore, previous oilflow studies indicate vorticity at the foot of a terminal normal shock for a 30° cone-cylinder configuration (Fig. 11).[13] The present results should, then, also exhibit a similar vortical flow in the separated region.

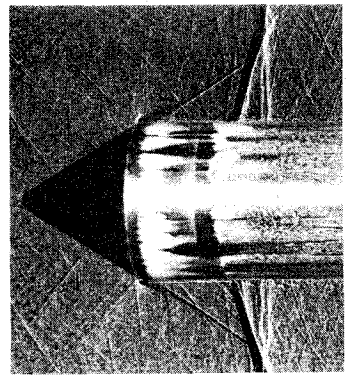

Fig. 11 Oilflow-shadowgraph photograph 30° cone-cylinder, $M = 0.9$, $\alpha = 0$.

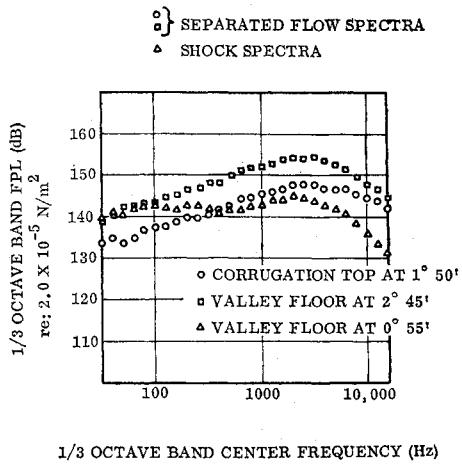

Fig. 12 Circumferential variation of fluctuating pressure spectra, $M = 0.8$, $\alpha = 0$, $x/c = 1.104$.

A possible indication of such vorticity from the present results is evident in the circumferential variation of spectra type. That is, at various circumferential positions, spectra typical of the separation shock and the separation bubble occur at the same axial station (Fig. 12). Likewise, comparison of the present over-all fluctuating pressure measurements reveals a circumferential rippling of the shock front (Fig. 13). It appears that the aft leg of the lambda shock is displaced periodically, while the fore-leg ripples. At $\phi = 2°\ 45'$ the shock lambda extends from $x/c = 1.13$ to 1.26, while at $\phi = 3°\ 40'$ the lambda extends from $x/c = 1.13$ to 1.21. Likewise, the forward edge of the lambda goes from $x/c = 1.104$ to 1.13 between $\phi = 55'$ and $\phi = 1°\ 45'$. (It should be noted that the transducer diameter was approximately 0.0029 c; thus, differences of a few hundredths of c are readily measureable.)

These results tend to support the postulation that the separation pocket is three-dimensional The cellular flow model sketched in Fig. 14, is therefore proposed. This model is consistent with many independent observations. The flow between the cells is turned back by the displaced aft leg of the lambda shock. It is then swept forward to the center of the cell by the adjacent vortex. A cut through the center of the cell would reveal a recirculatory flow very similar to the conventional two-dimensional recirculation region (with Trilling's resonance), except that the returning flow is scavenged through the counter-rotating vortices which vent the separation pocket. These vortices are eventually turned downstream longitudinally. The existence of the longitudinal vorticity is verified by the circumferential variation of the boundary-layer displacement thickness aft of separation (Fig. 15). Zakkay and Calarese have shown such boundary-layer waviness to be evidence of streamwise vorticity.[20] These streamwise vortices may be the mechanism for convecting the pressure fluctuations due to resonance of a separation pocket downstream to affect the pressure fluctuations in a following pocket as observed on the biconic nose (Fig. 9).

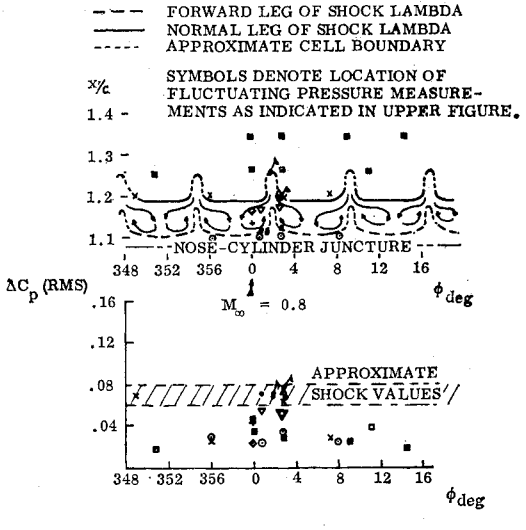

Fig. 13 Evidence of shock rippling from fluctuating pressure measurements, $M = 0.8$, $\alpha = 0$.

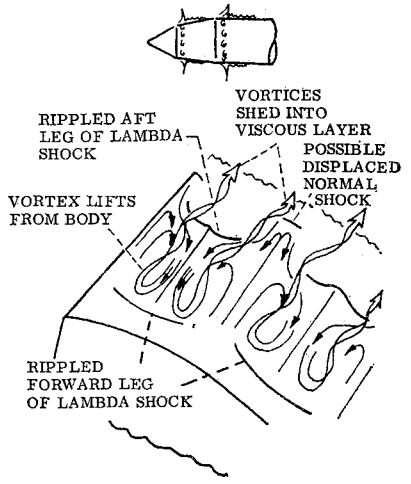

Fig. 14 Postulated flow model

Conclusions

Fluctuating pressure and boundary-layer profile measurements under the foot of the normal shock aft of the shoulder of three nose-cylinder bodies indicate a complicated, interactive, flowfield. The salient results can be summarized as follows: 1) a resonance of the separation pocket that is reasonably well predicted by Trilling's two-dimensional incident shock model; 2) a shock front that is rippled circumferentially; and 3) a rippled boundary layer aft of separation.

A three-dimensional flow model is proposed which consists of cells of two-dimensional flow vented by pairs of vortices. The model accounts for the observed characteristics of separated region and is consistent with existing pervasive evidence of vorticity in regions of separated flow.

The vortical nature of the separated flow provides a mechanism for both streamwise and transverse fluctuating pressure correlations. The shed vorticity prescribes a mechanism whereby successive pockets of flow separation may be coupled. The concave flow in regions of separation will magnify the preexisting vorticity; thus the vortices produced in a forward region of separation (and their alteration by local flow conditions) may set the vortex pattern in successive regions of separation.

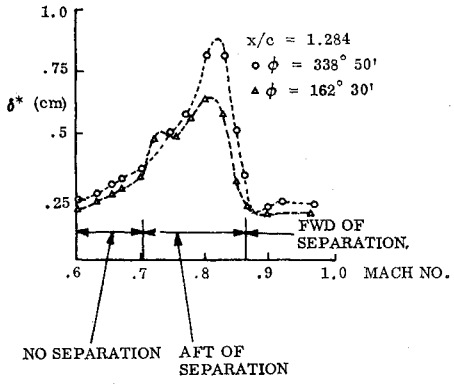

Fig. 15 Evidence of boundary layer waviness aft of reattachment, 15° cone-cylinder, $\alpha = 0$.

References

[1] Bendat, J. S. and Piersol, A. G., *Measurement and Analysis of Random Data*, Wiley, New York, 1966, p. 33.

[2] *Test Facilities Handbook*, Arnold Engineering Development Center, Arnold Air Force Station, Tenn., July 1971.

[3] Lankston, M., "Aerodynamic Model Test Report, T III M, Final Test Report, 5.35T Force & Pressure Test," SSD-CR-66-683, Dec. 1966, Martin Co., Denver, Colo.

[4] Coe, C. F. and Kaske, A. J., "The Effects of Nose Bluntness on the Pressure Fluctuations Measured on 15° and 20° Cone-cylinders at Transonic Speeds," TM-X779, June 1963, NASA.

[5] Ericsson, L. E., "Aeroelastic Instability Caused by Slender Payloads," *Journal of Spacecraft and Rockets*, Vol. 4, No. 1, Jan. 1967, pp. 65–73.

[6] Chevalier, H. L. and Robertson, J. E., "Pressure Fluctuations Resulting from an Alternating Flow Separation and Attachment at Transonic Speeds," TDR 63-204, Nov. 1963, Arnold Engineering Development Center, Arnold Air Force Station, Tenn.

[7] Coe, C. F. and Nute, J. B., "Steady and Fluctuating Pressure at Transonic Speeds on Hammerhead Launch Vehicles," TM X-778, Dec. 1962, NASA.

[8] Trilling, L., "Oscillatory Shock Boundary Layer Interaction," *Journal of Aeronautical Sciences*, Vol. 25, No. 5, May 1958, pp. 301–304.

[9] Ordway, D. E. and Lyons, J. M., "Ground Wind Induced Resonance of Launch Vehicles," *Transactions of the Eighth Symposium on Ballistic Missile and Space Technology*, Vol. VI, Oct. 16–18, 1963, San Diego, Calif.

[10] Ginoux, J. J., "Experimental Evidence of Three-Dimensional Perturbations and Reattachment of a Two-Dimensional Laminar Boundary Layer at $M = 2.05$," TN-1, 1958, Training Center for Experimental Aerodynamics, Belgium.

[11] Roshko, A. and Thomke, G. J., "Observations of Turbulent Reattachment Behind an Axisymmetric Downstream-Facing Step in Supersonic Flow," *AIAA Journal*, Vol. 4, No. 6, June 1966, pp. 975–980.

[12] Reding, J. P., Guenther, R. A., Ericsson, L. E., and Leff, A. D., "Nonexistence of Axisymmetric Separated Flow," *AIAA Journal*, Vol. 7, No. 7, July 1969, pp. 1374–1375.

[13] Ericsson, L. E., Reding, J. P., and Guenther, R. A., "Analytic Difficulties in Predicting Dynamic Effects of Separated Flow," *Journal of Spacecraft and Rockets*, Vol. 8, No. 8, Aug. 1971, pp. 872–878.

[14] Uebelhack, H. T., "Turbulent Flow Separation Ahead of Forward Facing Steps in Supersonic Two-Dimensional and Axisymmetric Flow," TN54, July 1969, von Kármán Inst. for Fluid Dynamics, Rhode-Saint-Genese, Belgium.

[15] Gersten, K. and Steinheuser, J., "Untersuchungen im Institut für Aerodynamik auf dem Gebiet der Grenzschichtströmungen," *DFL-Mitteilungen*, Heft 7, 1967, pp. 311–328.

[16] Ginoux, J. J., "On some Properties of Reattaching Laminar and Transitional High Speed Flows," TN 53, Sept. 1969, von Kármán Inst. for Fluid Dynamics, Rhode-Saint-Genese, Belgium.

[17] Tobak, M., "Hypothesis for the Origin of Cross-Hatching," *AIAA Journal*, Vol. 8, No. 2, Feb. 1970, pp. 330–334.

[18] Persen, L. N., "Exploratory Experiments in Water on Stream-Wise Vortices and Crosshatching of the Surface of Reentry Bodies," ARL-69 0160, Sept. 1969, Aerospace Reaserch Lab., Wright-Patterson Air Force Base, Ohio.

[19] Persen, L. N., "Investigation of Streamwise Vortex Systems Generated in Certain Classes of Curved Flow," ARL 68-0134, July 1968, Aerospace Research Lab. Wright-Patterson Air Force Base, Ohio.

[20] Zakkay, V. and Calarese, W., "An Experimental Investigation of Vortex Generation in a Turbulent Boundary Layer Undergoing Adverse Pressure Gradient," NASA CR-2037, June 1972, New York Univ., New York.